Gas-Phase Reactions of Transition-Metal Ions with Molecular Oxygen: Room-Temperature Kinetics and Periodicities in Reactivity

Gregory K. Koyanagi, Doina Caraiman, Voislav Blagojevic, and Diethard K. Bohme*

Department of Chemistry, Centre for Research in Mass Spectrometry and Centre for Research in Earth and Space Science, York University, Toronto, Ontario, Canada, M3J 1P3

An Inductively-Coupled Plasma/Selected-Ion Flow Tube (ICP/SIFT) tandem mass spectrometer has been employed in a systematic survey of room- temperature reactions of O_2 with 29 transition-metal ions. The atomic ions are produced at ca. 5500 K in an ICP source and are allowed to decay radiatively and to thermalize by collisions with Ar and He atoms prior to reaction. Rate coefficients were measured for the reactions of first-row atomic ions from Sc^+ to Zn^+, of second-row atomic ions from Y^+ to Cd^+ (excluding Tc^+) and of third-row atomic ions from La^+ to Hg^+. Both O-atom abstraction and O_2 addition were observed as primary reaction channels. Periodicities in reactivity are identified and are compared with periodicities in the O-atom affinity of the atomic ion. O-atom abstraction was observed to be efficient when exothermic and inefficient when endothermic. NbO^+, MoO^+, TaO^+, and WO^+ reacted further in a second O-atom transfer reaction with O_2. ReO_2^+ produced by direct addition of O_2 to Re^+ reacted further by both O-atom abstraction and O_2 addition. Sequential O_2 addition was observed to produce the higher oxides: MO_3^+ (M = Ti, V, Y, Zr, Hf, Os), MO_4^+ (M = Cr, Fe, Co, Ni, Cu, Nb, Mo, Ru, Rh, Hf, Ta, W, Re, Os, Ir, Pt, Au), MO_5^+ (M = V, Re, Os), MO_6^+ (M = Nb, W, Re) and MO_7^+ (M = V). Novel termolecular reactions second-order in oxygen were identified for Os^+ and ZrO^+ at high oxygen concentrations to produce O_2^+ and OsO^+ from Os^+ and a neutral metal oxide from Zr^+.

Introduction

The importance of transition metals in oxidation catalysis is now well-established, and there continues to be a need to understand the underlying chemistry. The case has been made that fundamental aspects of this chemistry can be elucidated with gas-phase measurements of the reactivity patterns for cations of transition-metals and their oxides.[1] Many such studies now have been reported for selected transition metals on the periodic table, the choice of the transition metal ion under experimentation being largely determined by the ease of its production.

Apparently, the first measurement of a reaction of a transition-metal ion with O_2 in the gas phase was that with Ti^+ reported in 1974 by Biondi et al.[2] Ti^+ ions were produced with a titanium−tungsten filament and the rate coefficient for the reaction with O_2 was measured in a drift-tube mass spectrometer over an energy range from thermal energies (300 K) to 2 eV (mean kinetic energy). In 1985, the drift tube was coupled to a zirconium-ion discharge containing $ZrBr_4$ to measure the rate coefficient for the reaction of Zr^+ with O_2 over a similar energy range.[3] Gas-phase reactions of transition metal ions with O_2 were first looked at systematically across the first row of the periodic table using ion cyclotron resonance (ICR) spectroscopy.[4] Qualitative measurements of a "go/no go" variety were reported for Ti^+, V^+, Cr^+, Mn^+, Fe^+, Co^+, and Cu^+ all of which were produced by laser ablation/ionization of the corresponding metal targets. These results demonstrated for the first time high reactivity for the early 1st-row transition-metal ions and low reactivity for the late 1st-row ions. More recently, all of the

1st-row transition metal ion reactions with O_2 have been scrutinized more closely in the energy range from near-thermal to about 10 eV (CM) using guided ion-beam techniques.[5] In these studies, the ions were produced by surface ionization at ca. 2200 K. Reactions with Sc^+, Ti^+, and V^+ were shown to be exothermic and fast near thermal energies, whereas the remaining 1st row ions exhibited endothermic behavior that provided measured O-atom affinities (for Cr^+, Mn^+, Fe^+, Co^+, Ni^+, Cu^+, and Zn^+).

In the work reported here, ions of all the 1st row, 2nd row (except Tc) and 3rd row transition elements have been generated in one source, an inductively coupled plasma (ICP). They were reacted with O_2 at room temperature in helium buffer gas ($P = 0.35 \pm 0.1$ Torr) using a Selected-Ion Flow Tube tandem mass spectrometer.[6,7] The results establish patterns in reactivity across and down the periodic table for the direct oxidation of the transition-metal ions and, in several cases, also the reactivities of transition metal-oxide ions with molecular oxygen to form higher oxides. Very recently, we have separately reported results obtained for the oxidation of atomic lanthanide cations with both O_2 and N_2O using a similar experimental approach.[8]

Experimental Method

The results reported here were obtained using the Selected-Ion Flow Tube (SIFT) tandem mass spectrometer in the Ion-Chemistry Laboratory at York University, described in detail elsewhere.[9,10] Recently, it has been modified to accept ions generated in an inductively coupled plasma (ICP) torch through an atmosphere/vacuum interface (ELAN series, Perkin-Elmer SCIEX). The ICP ion source and interface have also been described previously.[6,7] Solutions containing the metal salt of

* To whom correspondence should be addressed. E-mail: dkbohme@yorku.ca.

interest having concentration of ca. 5 μg l^{-1} were peristaltically pumped via a nebulizer into the plasma. The nebulizer flow was adjusted to maximize the ion signal detected downstream of the SIFT. The sample solutions were prepared using atomic spectroscopy standard solutions commercially available from SPEX, Teknolab, J. T. Baker Chemical Co., Fisher Scientific Company, Perkin-Elmer and Alfa Products. Aliquots of standard solutions were diluted with highly purified water produced in the Millipore Milli-Qplus ultrapure water system. The final concentrations were varied within 5−20 ppm interval to achieve suitable intensity of the resultant ion beam. Normally, a stabilizing agent was added to each solution to prevent precipitation. That was either HNO$_3$ or HCl for acid-stabilized salts or KOH for those base-stabilized.

The transition-metal ions emerge from the plasma at a nominal ion temperature of 5500 K with the Maxwell−Boltzmann state distributions given in Table 1. These were derived from available optical spectra[11,12] and are given for the two electronic spin states with the highest population at 5500 K. After extraction from the ICP, the plasma ions may experience both radiative electronic-state relaxation and collisional electronic-state relaxation. The latter may occur with argon as the extracted plasma cools upon sampling and then by collisions with He atoms in the flow tube (ca. 4×10^5 collisions) prior to the reaction region, but the actual extent of electronic relaxation (either radiative or collisional) is not known. The collisions with He ensure that the ions reach a translational temperature equal to the tube temperature of 295 $\pm$ 2 K prior to entering the reaction region. The helium buffer gas pressure was 0.35 ± 0.01 Torr. Reagent gases had purities better than 99.5%. Oxygen was introduced into the flow tube as a pure gas (>99.5%).

Reaction rate coefficients were determined in the usual manner using pseudo first-order kinetics.[9,10] The rate coefficients for the primary and consecutive reactions reported herein have an absolute accuracy of $\pm$30%. When rate coefficients are reported as an upper limit ($\leq$), this indicates the statistical scatter in the data was significant compared to the slope of the data and an upper limit (based on the line of steepest slope through the data) is reported.

Results and Discussion

The reactions of 29 different transition-metal ions were investigated with O$_2$. The results obtained for the reaction of the vanadium ions with O$_2$ have been reported separately.[13] Both the primary and the higher-order chemistry was monitored. Table 2 shows that the primary reactions exhibit a wide range in measured reaction rate coefficients from $< 10^{-14}$ to 5.0×10^{-10} cm^3 molecule^{-1} s^{-1}. Two different reaction channels were observed as indicated in reaction 1

$$M^+ + O_2 \rightarrow MO^+ + O \qquad (1a)$$

$$\rightarrow MO_2^+ \qquad (1b)$$
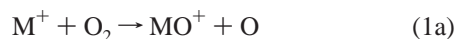
Bimolecular electron transfer is endothermic for all reactions investigated because the ionization energy of O$_2$ is quite high, IE(O$_2$) = 12.07 eV, higher than that of all of the transition metals.[14]

Ten of the 29 reactions investigated exhibited only the bimolecular O-atom transfer channel (1a) and were generally quite fast, $k \geq 7.5 \times 10^{-11}$ cm^3 molecule^{-1} s^{-1}. The remaining reactions were all quite slow ($k < 1 \times 10^{-12}$ cm^3 molecule^{-1} s^{-1}) and sixteen of these were observed to proceed only by O$_2$

TABLE 1: Electronic Configurations and Maxwell−Boltzmann Distributions for the Two States of Transition-Metal Ions with the Highest Population at 5500K

ion	term	config	pop. (%)	energy (eV)	no. of levels
Sc$^+$	^{3}D	4s^1 3d^1	64.7	0.0−0.22	3
	^{3}F	3d^2	18.4	0.60−0.62	3
Ti$^+$	^{4}F	4s^1 3d^2	44.0	0.0−0.05	4
	^{4}F	3d^3	35.1	0.11−0.15	4
V$^+$	^{5}D	3d^4	59.6	0.0−0.04	5
	^{5}F	4s^1 3d^3	29.3	0.32−0.39	5
Cr$^+$	^{6}S	3d^5	79.0	0.0	1
	^{6}D	4s^1 3d^4	16.3	1.48−1.55	5
Mn$^+$	^{7}S	4s^1 3d^5	83.7	0.0	1
	^{5}D	3d^6	8.9	1.77−1.85	5
Fe$^+$	^{6}D	4s^1 3d^6	61.6	0.0−0.12	5
	^{4}F	3d^7	29.4	0.23−0.39	4
Co$^+$	^{3}F	3d^8	56.1	0.0−0.20	3
	^{5}F	4s^1 3d^7	36.7	0.41−0.64	5
Ni$^+$	^{2}D	3d^9	81.2	0.0−0.19	2
	^{4}F	4s^1 3d^8	16.0	1.04−1.32	4
Cu$^+$	^{1}S	3d^{10}	99.1	0.0	1
	^{3}D	4s^1 3d^9	0.8	2.72−2.97	3
Zn$^+$	^{2}S	4s^1 3d^{10}	100	0.0	1
Y$^+$	^{1}S	5s^2	24.2	0.0	1
	^{3}D	5s^1 4d^1	54.4	0.10−0.18	3
Zr$^+$	^{4}F	5s^1 4d^2	44.0	0.0−0.16	4
	^{4}F	4d^3	11.9	0.32−0.47	4
Nb$^+$	^{5}D	4d^4	50.8	0.0−0.15	5
	^{5}F	5s^1 4d^3	25.8	0.29−0.51	5
Mo$^+$	^{6}S	4d^5	73.0	0.0	1
	^{6}D	5s^1 4d^4	14.0	1.46−1.67	5
Ru$^+$	^{4}F	4d^7	74.8	0.0−0.38	4
	^{4}P	4d^7	8.8	1.02−1.16	3
	^{6}D	5s^1 4d^6	9.1	1.13−1.44	5
Rh$^+$	^{3}F	4d^8	84.7	0.0−0.44	3
	^{1}D	4d^8	5.2	1.01	1
	^{3}P	4d^8	7.5	1.33−1.44	3
Pd$^+$	^{2}D	4d^9	100	0.0−0.44	2
Ag$^+$	^{1}S	4d^{10}	100	0.0	1
Cd$^+$	^{2}S	5s^1 4d^{10}	100	0.0	1
Ba$^+$	^{2}S	6s^1	66.0	0.0	1
	^{2}D	5d^1	33.4	0.60−0.70	2
La$^+$	^{3}F	5d^2	40.6	0.0−0.24	3
	^{3}D	6s^1 5d^1	26.6	0.23−0.40	3
Hf$^+$	^{2}D	6s^2 5d^1	54.0	0.0−0.38	2
	^{4}F	6s^1 5d^2	36.0	0.45−1.04	4
Ta$^+$	^{5}F	6s^1 5d^3	56.4	0.0−0.77	5
	^{3}P	6s^2 5d^2	16.6	0.51−0.70	3
W$^+$	^{6}D	6s^1 5d^4	76.8	0.0−0.76	5
	^{4}F	6s^1 5d^4	6.1	1.08−1.84	4
Re$^+$	^{7}S	6s^1 5d^5	85.7	0.0	1
	^{5}D	6s^2 5d^4	9.6	1.71−1.84	5
Ir$^+$	^{5}F^c	6s^1 5d^7	33.3	0.0	1
	^{3}F^d	5d^8	18.4	0.28	1
Pt$^+$	^{2}D	5d^9	70.9	0.0−1.04	2
	^{4}F	6s^1 5d^8	26.8	0.59−1.96	4
Au$^+$	^{1}S	5d^{10}	97.0	0.0	1
	^{3}D	6s^1 5d^9	2.9	1.86−3.44	3
Hg$^+$	^{2}D	6s^1 5d^{10}	100	0.0	1

^{a} Number of microstates (multiplets) with the same electronic configuration. ^{b} Only mixed spin states could be specified.[12] ^{c} Actual configuration: 89% (^{5}F), 10% (^{3}G). ^{d} Actual configuration: 90%(^{3}F),4% (^{1}G),3% (^{3}F) Energy levels as high as 3.7 eV were included in the calculations which were based on known optical spectra.[11] The data for Ir$^+$ was derived from ref 12. Os$^+$ is not shown since no suitable spectroscopic data could be found.

addition (channel (1b) while two others (Mn$^+$ and Cd$^+$) also were slow but showed no products in the flow regime investigated. Only the reaction with Hf$^+$ exhibited both channels (1a)) and (1b) in the proportion 93:7. In four cases (Nb$^+$, Mo$^+$, Ta$^+$, and W$^+$) the oxide ion produced in reaction 1a reacted further in a second O-atom transfer reaction with O$_2$.

TABLE 2: Rate Coefficients (in units of cm^3 molecule^{-1} s^{-1}) Measured for O-atom Transfer Reactions of Transition-Metal Ions, M$^+$, with Molecular Oxygen in Helium at 0.35 ± 0.01 Torr and 295 ± 2 K

primary reaction of M$^+$	k^a	$k_{cap}{}^b$	k/k_{cap}	MO$_x^{+,c}$
Sc$^+$ + O$_2$ → ScO$^+$ + O	3.7 × 10^{-10}	6.8 × 10^{-10}	0.54	
Ti$^+$ + O$_2$ → TiO$^+$ + O	4.6 × 10^{-10}	6.75 × 10^{-10}	0.68	TiO$_3^+$
V$^+$ + O$_2$ → VO$^+$ + O	2.8 × 10^{-10}	6.7 × 10^{-10}	0.42	VO$_3^+$,VO$_5^+$,VO$_7^+$
Cr$^+$ + O$_2$ → CrO$_2^+$	2.2 × 10^{-13}	6.6 × 10^{-10}	3.0 × 10^{-4}	
Mn$^+$ + O$_2$ → NR	<1.0 × 10^{-14}	6.6 × 10^{-10}	<1.5 × 10^{-5}	
Fe$^+$ + O$_2$ → FeO$_2^+$	4.3 × 10^{-13}	6.6 × 10^{-10}	6. 5 × 10^{-4}	FeO$_4^+$
Co$^+$ + O$_2$ → CoO$_2^+$	1.5 × 10^{-13}	6.5 × 10^{-10}	2.3 × 10^{-4}	CoO$_4^+$
Ni$^+$ + O$_2$ → NiO$_2^+$	2.0 × 10^{-13}	6.5 × 10^{-10}	3.1 × 10^{-4}	NiO$_4^+$
Cu$^+$ + O$_2$ → CuO$_2^+$	2.4 × 10^{-13}	6.4 × 10^{-10}	3.8 × 10^{-4}	CuO$_4^+$
Zn$^+$ + O$_2$ → ZnO$_2^+$	2.0 × 10^{-13}	6.4 × 10^{-10}	3.1 × 10^{-4}	
Y$^+$ + O$_2$ → YO$^+$ + O	4.1 × 10^{-10}	6.1 × 10^{-10}	0.67	YO$_3^+$
Zr$^+$ + O$_2$ → ZrO$^+$ + O	5.0 × 10^{-10}	6.1 × 10^{-10}	0.82	ZrO$_3^+$
Nb$^+$ + O$_2$ → NbO$^+$ + O	4.3 × 10^{-10}	6.0 × 10^{-10}	0.72	NbO$_2^+$, NbO$_4^+$, NbO$_6^+$
Mo$^+$ + O$_2$ → MoO$^+$ + O	7.5 × 10^{-11}	6.0 × 10^{-10}	0.13	MoO$_2^+$, MoO$_4^+$
Ru$^+$ + O$_2$ → RuO$_2^+$	1.7 × 10^{-13}	6.0 × 10^{-10}	2.8 × 10^{-4}	RuO$_4^+$
Rh$^+$ + O$_2$ → RhO$_2^+$	9.2 × 10^{-14}	6.0 × 10^{-10}	1.5 × 10^{-4}	RhO$_4^+$
Pd$^+$ + O$_2$ → PdO$_2^+$	9.1 × 10^{-14}	5.95 × 10^{-10}	1.5 × 10^{-4}	
Ag$^+$ + O$_2$ → AgO$_2^+$	1.0 × 10^{-13}	5.9 × 10^{-10}	1.7 × 10^{-4}	
Cd$^+$ + O$_2$ → NR	< 1.0 × 10^{-14}	5.9 × 10^{-10}	< 1.7 × 10^{-5}	
La$^+$ + O$_2$ → LaO$^+$ + O	4.3 × 10^{-10}	5.8 × 10^{-10}	0.74	
Hf$^+$ + O$_2$ → HfO$^+$ + O	4.1 × 10^{-10}	5.7 × 10^{-10}	0.67	HfO$_3^+$, HfO$_4^+$
→ HfO$_2^+$ (7%)				
Ta$^+$ + O$_2$ → TaO$^+$ + O	4.7 × 10^{-10}	5.7 × 10^{-10}	0.82	TaO$_2^+$, TaO$_4^+$,TaO$_6^+$
W$^+$ + O$_2$ → WO$^+$ + O	4.4 × 10^{-10}	5.6 × 10^{-10}	0.79	WO$_2^+$, WO$_4^+$, WO$_6^+$
Re$^+$ + O$_2$ → ReO$_2^+$	1.1 × 10^{-12}	5.6 × 10^{-10}	2.0 × 10^{-3}	ReO$_3^+$, ReO$_4^+$,ReO$_5^+$, ReO$_6^+$
Os$^+$ + O$_2$ → OsO$_2^+$	3.7 × 10^{-12}	5.6 × 10^{-10}	6.6 × 10^{-3}	OsO$_3^+$, OsO$_4^+$ OsO$_5^+$
Ir$^+$ + O$_2$ → IrO$_2^+$	1.3 × 10^{-13}	5.6 × 10^{-10}	2.3 × 10^{-4}	IrO$_4^+$
Pt$^+$ + O$_2$ → PtO$_2^+$	1.6 × 10^{-13}	5.6 × 10^{-10}	2.9 × 10^{-4}	PtO$_4^+$
Au$^+$ + O$_2$ → AuO$_2^+$	1.2 × 10^{-13}	5.6 × 10^{-10}	2.1 × 10^{-4}	AuO$_4^+$
Hg$^+$ + O$_2$ → HgO$_2^+$	2.4 × 10^{-13}	5.6 × 10^{-10}	4.3 × 10^{-4}	

^{a} Estimated uncertainty is ±30%. ^{b} Collision rate coefficient calculated using the algorithm of the modified variational transition-state/classical trajectory theory developed by Su and Chesnavich.[15] ^{c} Other metal-oxide ions observed to be formed with higher-order chemistry.

TABLE 3: Experimental O-Atom Affinities, D_0(M$^+$−O) in kcal mol^{-1}, for the Transition-Metal Ions Taken from the Review by Schröder et al.[1]

Sc$^+$	164.6 ± 1.4^a	Y$^+$	167.0 ± 4.2^b	La$^+$	206 ± 4^d
Ti$^+$	158.6 ± 1.6^a	Zr$^+$	178.9± 2.5^b	Hf$^+$	173 ± 5^e
V$^+$	134.9 ± 3.5^a	Nb$^+$	164.4 ± 2.5^b	Ta$^+$	188 ± 15^e
Cr$^+$	85.8 ± 2.8^a	Mo$^+$	116.7± 0.5^b	W$^+$	126 ± 10^e
Mn$^+$	68.0 ± 3.0^a			Re$^+$	115 ± 15^f
Fe$^+$	80.0 ± 1.4^a	Ru$^+$	87.9 ± 1.2^c	Os$^+$	100 ± 12^g
Co$^+$	74.9 ± 1.2^a	Rh$^+$	69.6 ± 1.4^c	Ir$^+$	59^e
Ni$^+$	63.2 ± 1.2^a	Pd$^+$	33.7 ± 2.5^c	Pt$^+$	77^h
Cu$^+$	37.4 ± 3.5^a	Ag$^+$	28.4 ± 1.2^c		
Zn$^+$	38.5 ± 1.2^a				

^{a} ref 16. ^{b}ref 17. ^{c}ref 18. ^{d}ref 19. ^{e}ref 14. ^{f}ref 20. ^{g}ref 21. ^{h}ref 22.

Table 2 summarizes the measured rate coefficients, calculated reaction efficiencies and the observed higher-order chemistry. The reaction efficiency is taken to be equal to the ratio k/k_c where k is the experimentally measured rate coefficient and k_c is the capture or collision rate coefficient computed using the algorithm of the modified variational transition-state/classical trajectory theory developed by Su and Chesnavich.[15] Figure 1 displays these data on a periodic table.

Monoxide Formation by Oxygen-Atom Transfer. O-atom transfer, reaction 1a, was observed with Group 3B (Sc$^+$, Y$^+$, La$^+$), 4B (Ti$^+$, Zr$^+$, Hf$^+$), 5B (V$^+$, Nb$^+$, Ta$^+$) and 6B (Mo$^+$ and W$^+$, but not Cr$^+$) transition-metal ions. The rate coefficients measured for O-atom transfer are in the range 7.5 × 10^{-11} (for Mo$^+$) to 5.0 × 10^{-10} (for Zr$^+$) cm^3 molecule^{-1} s^{-1}. Figures 2 to 4 show measured ion profiles for first-row, second-row, and third-row ions that exhibit primary O-atom transfer (with the exception of Cr$^+$).

The O-atom affinity of O is quite high, OA(O) = 119.1 ± 0.1 kcal mol^{-1},[14] so that the formation of the monoxide cation

by reaction 1a can be expected to be exothermic for only those atomic ions with a comparable or higher O-atom affinity. Table 3 provides a listing of available experimental O-atom affinities[16−22] for the atomic ions investigated in this study and compiled in the review by Schröder et al.[1] Figure 1 shows the periodic variation of this affinity along with the variation of reaction efficiency. It is immediately obvious from Figure 1 that O-atom transfer from O$_2$ is exothermic only for the early transition-metal ions. Also, a strong correlation is evident from Figure 1 between the efficiency and exothermicity. The efficiency for O-atom transfer is high (>0.4) when exothermic and low (<0.1) when endothermic. The Group 6 atomic ions show an intermediate behavior as they are nearly thermoneutral. Figure 5 displays the overall dependence of the efficiency of O-atom transfer on the O-atom affinity of the metal ion.

Our rate coefficients for the O-atom transfer reactions of Ti$^+$ and Zr$^+$, (4.6 ± 1.4) × 10^{-10} and (5.0 ± 1.5) × 10^{-10} cm^3 molecule^{-1} s^{-1} respectively, are in excellent agreement with the early drift-tube mass spectrometer values of (5 ± 1) × 10^{-10} and (5.5 ± 0.3) × 10^{-10} cm^3 molecule^{-1} s^{-1}, respectively.[2,3] The kinetics for reactions of O$_2$ with most of the first-row transition-metal ions (Ti$^+$ to Cu$^+$ excluding Ni$^+$) have been investigated qualitatively by Kappes and Staley using ion cyclotron resonance (ICR) mass spectrometry.[4] The results obtained by these authors indicated the occurrence of reaction 1a for Ti$^+$ and V$^+$ and its nonoccurrence with Cr$^+$, Mn$^+$, Fe$^+$, Co$^+$, and Cu$^+$. These results are consistent with our measurements. Fisher et al. have explored the reactions of the first-row transition-metal ions Sc$^+$ to Zn$^+$ with O$_2$ using ion-beam mass spectrometry and have found that reaction 1a is exothermic and fast near thermal energies for Sc$^+$, Ti$^+$, and V$^+$ and endothermic and slow for the remaining metal ions.[5] The periodicity in
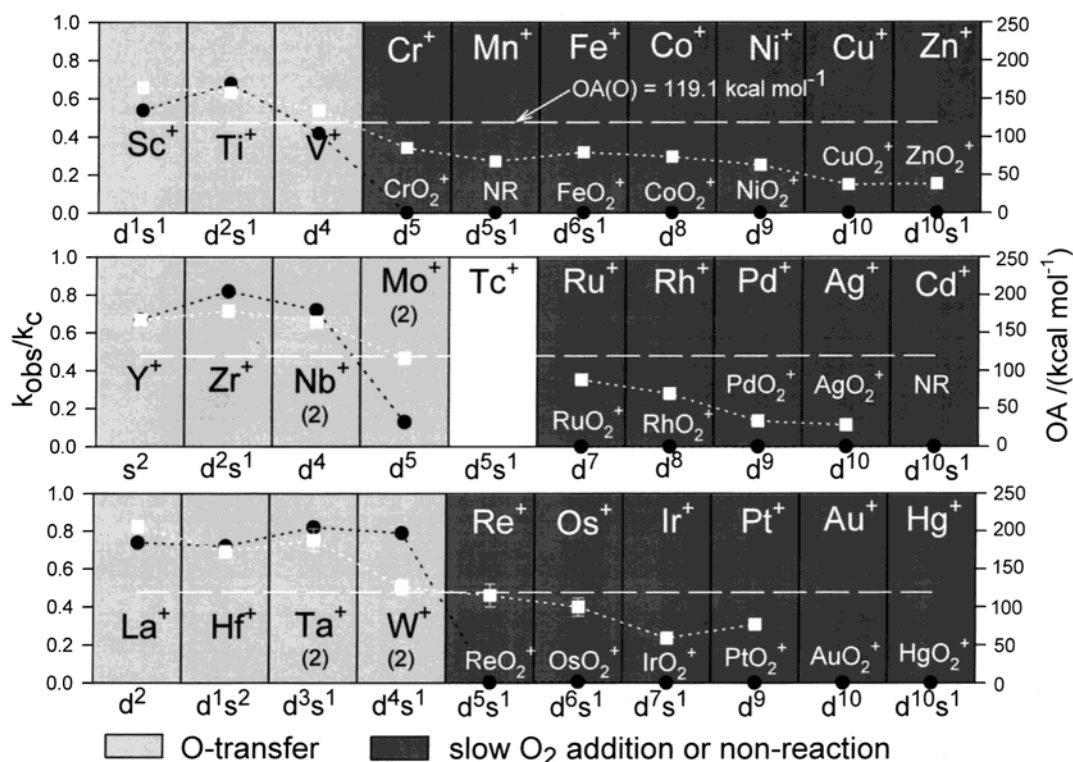
Figure 1. Periodic variations observed in the reactivities of transition-metal ions toward molecular oxygen, k_{obs}/k_c (represented as solid circles), and their O-atom affinities, OA (represented as open squares). k_{obs} represents the measured reaction rate coefficient and k_c is the calculated collision rate coefficient (see Table 1). Also indicated are the observed reaction channels (the number in parentheses indicates the number of sequential O-atom transfer reactions that were observed), the OA(O) line and the electronic configuration of the atomic ion. NR designates no reaction.

O-atom affinity of the first row metal ions (Ca^+ to Zn^+) was also obtained by these authors and discussed in detail. Again, these results are consistent with our room-temperature measurements.

Dioxide Formation by Sequential Oxygen-Atom Abstraction. A second O-atom abstraction, reaction 2, was observed only with the Group 5B ions Nb^+ and Ta^+ and the Group 6B ions Mo^+ and W^+ (see Figures 3 and 4).

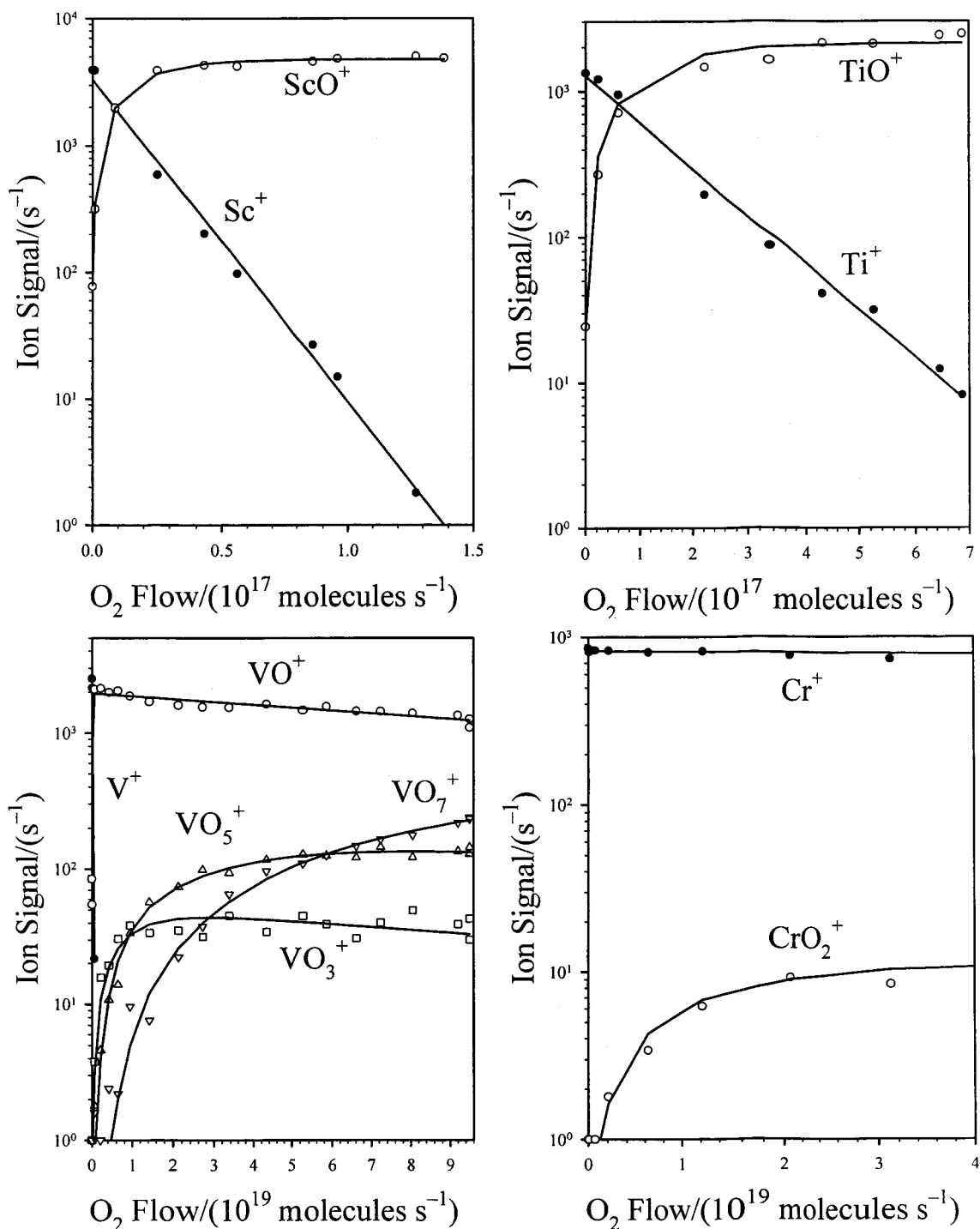$$MO^+ + O_2 \rightarrow MO_2^+ + O \qquad (2)$$
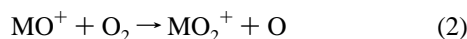
The rate coefficients measured for these reactions are shown in Table 4 along with calculated reaction efficiencies. All 4 of these reactions are rapid, $k \geq 3.7 \times 10^{-10}$ and efficient, $k/k_{cap} \geq 0.63$. The rate coefficient for the nonobserved second O-atom abstraction for the remaining transition-metal oxide ions can be assigned an upper limit of ca. 1×10^{-12} cm^3 molecule^{-1} s^{-1}.

These results are consistent with what is known about the O-atom affinities of transition-metal oxide cations that also have been reviewed by Schröder et al.[1] The Group 3 oxides ScO^+, YO^+, and LaO^+ have O-atom affinities (40, 41, and 23 kcal mol^{-1}, respectively) that are much lower than OA(O) = 119 kcal mol^{-1} and so are those for the Group 4 oxides TiO^+ (81 kcal mol^{-1}) and ZrO^+ (89 kcal mol^{-1}) and the Group 5 oxide VO^+ (90 kcal mol^{-1}). OA(HfO$^+$) apparently is not known. Of the oxide ions observed to be produced in reaction 1a only NbO^+ (132 kcal mol^{-1}), TaO^+ (140 kcal mol^{-1}), MoO^+ (128 kcal mol^{-1}) and WO^+ (132 kcal mol^{-1}) have known OAs higher than that of atomic oxygen.

The structure of the MO_2^+ ions formed in reaction 2 is uncertain as three isomers are possible: an inserted dioxide with OMO connectivity, OMO^+, an end-on coordinated O_2 ligand with a superoxide-like MOO structure, $M(OO)^+$, and a side-on
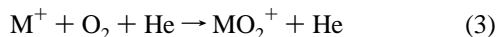
structure with an intact O_2 moiety, $M(O_2)^+$. Our own multi-collision technique,[23] which involves simply raising the nose-cone potential of the sampling nose cone did not yield bond cleavage for MO_2^+ ions and so did not provide bond-connectivity information. See, for example, the CIDs displayed in Figure 6 that illustrate the high stabilities of WO_2^+, TaO_2^+, and NbO_2^+. However, for some metals there exists separate information about the relative energies of various dioxide isomers with different bond connectivities. For example, Harvey et al.[24] have argued on the basis of the known thermochemistry of oxide formation and on the basis of NbO_2^+ reactivity measurements for NbO_2^+ ions produced by successive O-atom abstraction in a mixture of O_2 and N_2O that NbO_2^+ has the dioxide structure in its lowest-energy state. Therefore, we propose that this is the dioxide ion most likely to be formed in the reaction of NbO^+ with O_2 observed in our experiments. The sequential oxidation of Zr^+ with O_2 in a flow tube using a dc discharge source for Zr^+ has been achieved previously by Sievers and Armentrout.[25] These authors also report experimental results for the Xe collision-induced dissociation of ZrO_2^+ produced in this fashion. Only O-atom loss was observed and this is consistent with a dioxide OZr^+-O connectivity within ZrO_2^+ produced in their experiment and which therefore also should be formed in our experiments. MoO_2^+ has been produced previously by allowing Mo^+ to react sequentially with O_2 and both experiment and theory have indicated a very high value for D(OMo$^+$$-$O).[26,27] Values of 122 ± 13 kcal mol^{-1} and 131 ± 5 kcal mol^{-1} have been derived from known thermochemistry and observations of O-atom transfer and CASPT2Drel theory has provided a value of 120.8 kcal mol^{-1}.[26] Guided-ion beam mass spectrometry has provided values consistent with 131 ± 5 kcal mol^{-1}.[27]

Dioxide Formation by O_2 Addition. Slow, exclusive addition of O_2 was observed with the first-row ions Cr^+, Fe^+, Co^+,

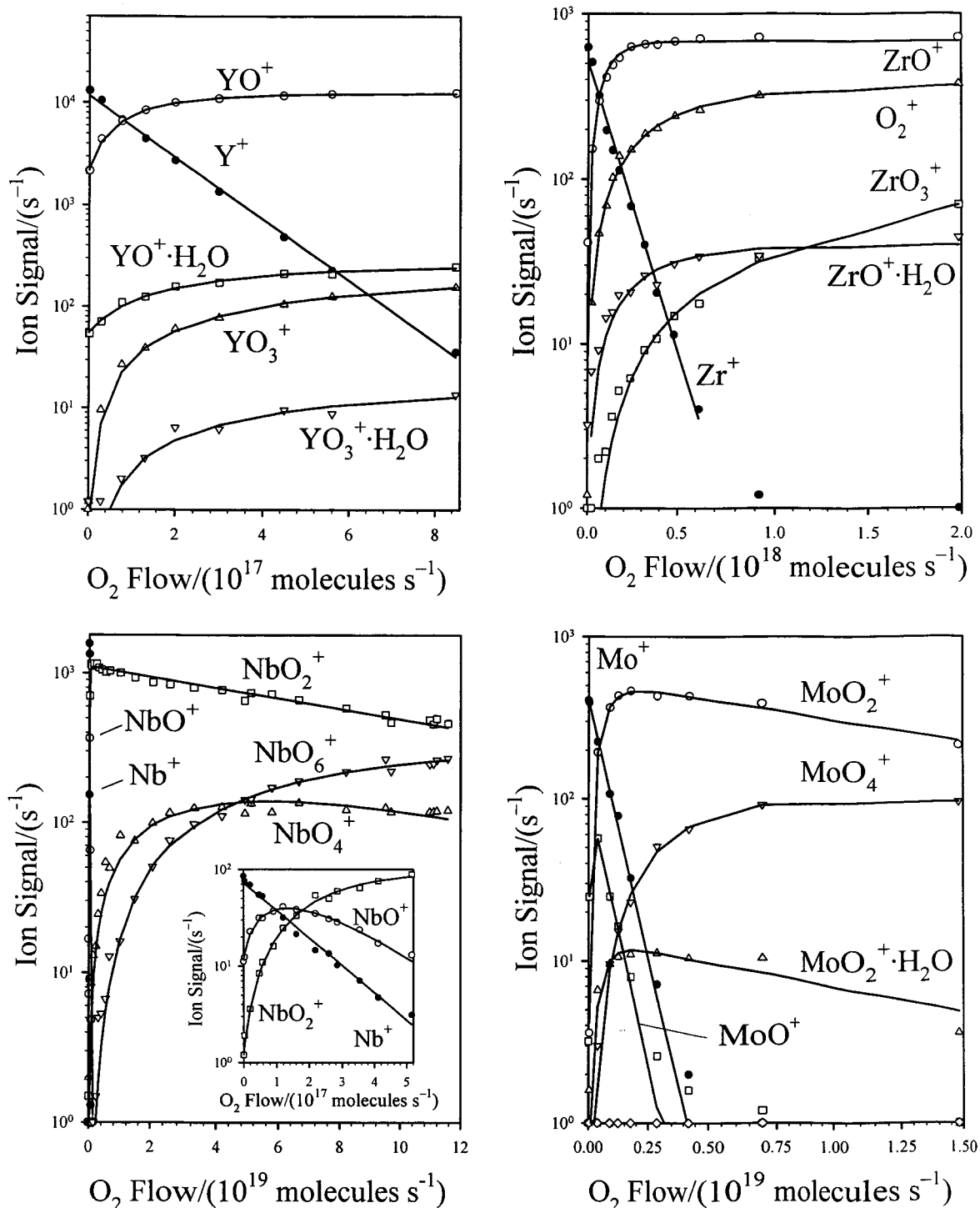RT Kinetics and Periodicities in Reactivity

J. Phys. Chem. A, Vol. 106, No. 18, 2002 **4585**

Figure 2. Composite of ICP/SIFT results for the reactions of the early first-row transition-metal ions Sc^+, Ti^+, V^+, and Cr^+ with O_2 in helium buffer gas at 0.35 ± 0.01 Torr and 295 ± 2 K.

Ni^+, Cu^+, and Zn^+, the second-row ions Ru^+, Rh^+, Pd^+, and Ag^+, and the third-row ions Re^+, Os^+, Ir^+, Pt^+, Au^+, and Hg^+. These are presumed to occur by the collisional stabilization reaction 3 at 0.35 Torr of He rather than by radiative association

$$M^+ + O_2 + He \rightarrow MO_2^+ + He \qquad (3)$$

(but pressure dependent studies were not performed). No reactions or products were observed with Mn^+ and Cd^+ in the flow regime investigated. A possible reason for this lower efficiency of addition is a lower O_2 binding energy. Mn^+ (d^5s^1) is expected to be anomalously stable because of the half-filled d shell. Table 2 includes a summary of the rate coefficients for the observed O_2 addition reactions.

The structures of the MO_2^+ dioxide ions formed directly by the addition of O_2 to M^+ also are not known and, again, our CID experiments did not help out in this regard. Various attempts have been made in the literature to describe the interaction of M^+ ions with O_2 theoretically. For example, a potential energy hypersurface for the reaction of $Fe^+(^6D)$ with O_2 ($^3\Sigma_g^-$) leading to the formation of $Fe(O_2)^+$ ($^6A_1$) or $OFeO^+$ ($^6A_1$) has been reported by Schröder et al.[28] These two isomers have the same multiplicity and symmetry and are close in energy (within ca. 5 kcal mol^{-1}). A barrier was found for the isomerization of $Fe(O_2)^+$ to $OFeO^+$ that lies well below the initial energy of the reactants. The hypersurface reported by Fiedler et al. for ground-state reaction of Cr^+ (^6S) with O_2 ($^3\Sigma_g^-$)
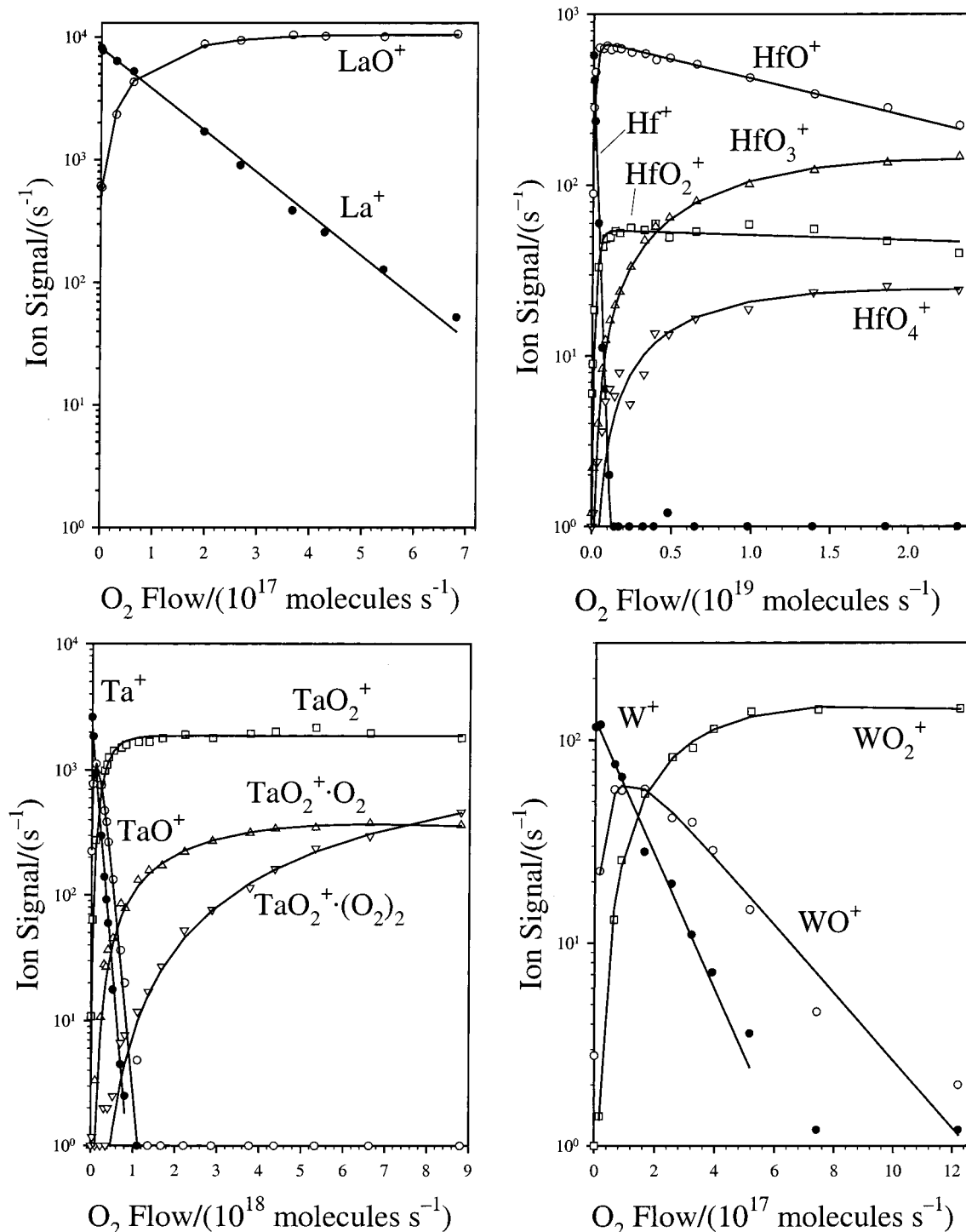
Figure 3. Composite of ICP/SIFT results for the reactions of the early second-row transition-metal ions Y^+, Zr^+, Nb^+, and Mo^+ with O_2 in helium buffer gas at 0.35 ± 0.01 Torr and 295 ± 2 K.

also is attractive for the formation of an $Cr(O_2)^+$ ion.[29] But in this case, a direct activation of O_2 ($^3\Sigma_g^-$) to form $OCrO^+$ ($^2A_1$) is not expected to occur at thermal energies because of the nature of the surface crossings that must occur for this to happen. The theoretical characterization of the PtO_2^+ potential energy surface also has been attempted but the results obtained by Brönstrup et al. are less certain and very dependent on the level of theory.[28] The CASPT2 calculations predict the doublet dioxide ion, ^{2}-$OPtO^+$, to be the global minimum and to lie some 25 kcal mol^{-1} below the superoxide structure, $^2PtOO^+$, although the nature of potential-energy surface for the possible isomerization of $^2PtOO^+$ to $^2OPtO^+$ is unclear. A binding energy of 30 ± 3 kcal

mol^{-1} is computed for $D(Pt^+-O_2)$ with respect to the peroxide ion.[30]

Higher Oxide Formation by O_2 Addition to Monoxide and Dioxide Ions. Large amounts of O_2 (up to 10^{20} molecules s^{-1}) were added into the flow tube in many experiments to explore higher-order oxide formation of which much was observed. The effective bimolecular rate coefficients that were determined from kinetic fits to the observed profiles are summarized in Table 5 along with effective efficiencies for O_2 addition under SIFT conditions.

A second O_2 addition was observed to form the tetroxide cation according to reaction 4 for M = Fe, Co, Ni, Cu, Nb,

RT Kinetics and Periodicities in Reactivity

J. Phys. Chem. A, Vol. 106, No. 18, 2002 **4587**

Figure 4. Composite of ICP/SIFT results for the reactions of the early third-row transition-metal ions La$^+$, Hf$^+$, Ta$^+$, and W$^+$ with O$_2$ in helium buffer gas at 0.35 ± 0.01 Torr and 295 ± 2 K.
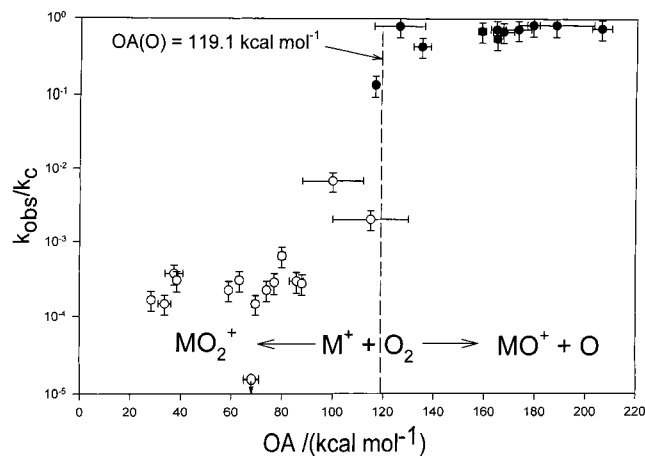
Mo, Ru, Rh, Hf, Ta, Re, Os, Ir, Pt, and Au

$$MO_2^+ + O_2 + He \rightarrow MO_4^+ + He \qquad (4)$$

Of these, MO$_4^+$ formation with M = Ni, and Os were the more efficient (>1%) suggesting higher stabilities for these tetroxide cations.

O$_2$ addition was also observed with some of the metal oxide ions according to reaction 5. Such reactions were observed for the early transition-metal ions,

$$MO^+ + O_2 + He \rightarrow MO_3^+ + He \qquad (5)$$

specifically the 1st row oxide ions TiO$^+$ and VO$^+$, the 2nd row oxide ions YO$^+$ and ZrO$^+$ and the 3rd row oxide ions HfO$^+$ and OsO$^+$, but with relatively low efficiencies. We have reported previously that VO$^+$ sequentially forms VO$_3^+$, VO$_5^+$ and VO$_7^+$ in the presence of oxygen under SIFT conditions and also have provided a detailed theoretical examination of their energies and possible structures.[13]

Finally, O$_2$ also was observed to add to MO$_2^+$ formed by two sequential O atom transfers to M$^+$. This is the case for M = Nb, Mo, Ta, and W. The higher oxides formed include NbO$_4^+$, NbO$_6^+$, MoO$_4^+$, TaO$_4^+$, TaO$_6^+$, and WO$_4^+$. Multicol-

4588 *J. Phys. Chem. A, Vol. 106, No. 18, 2002*

Koyanagi et al.

Figure 5. Semilogarithmic dependence of the reactivity of transition-metal ions toward molecular oxygen, k_{obs}/k_c, on their O-atom affinities, OA. k_{obs} represents the measured reaction rate coefficient and k_c is the calculated collision rate coefficient (see Table 1). Reactions on the right of the dashed line are exothermic, whereas those on the left are endothermic.

TABLE 4: Rate Coefficients (in units of cm^3 molecule^{-1} s^{-1}) Measured for O-atom Transfer Reactions of Transition-metal Oxide Ions with Molecular Oxygen in Helium at 0.35 ± 0.01 Torr and 295 ± 2 K
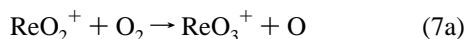
reaction	k	$k_{cap}{}^a$	k/k_{cap}
$NbO^+ + O_2 \rightarrow NbO_2^+ + O$	4.1×10^{-10}	5.9×10^{-10}	0.69
$MoO^+ + O_2 \rightarrow MoO_2^+ + O$	5.8×10^{-10}	5.9×10^{-10}	0.98
$TaO^+ + O_2 \rightarrow TaO_2^+ + O$	4.0×10^{-10}	5.6×10^{-10}	0.71
$WO^+ + O_2 \rightarrow WO_2^+ + O$	4.6×10^{-10}	5.6×10^{-10}	0.82

^{a} Collision rate coefficient calculated using the algorithm of the modified variational transition-state/classical trajectory theory developed by Su and Chesnavich.[15]
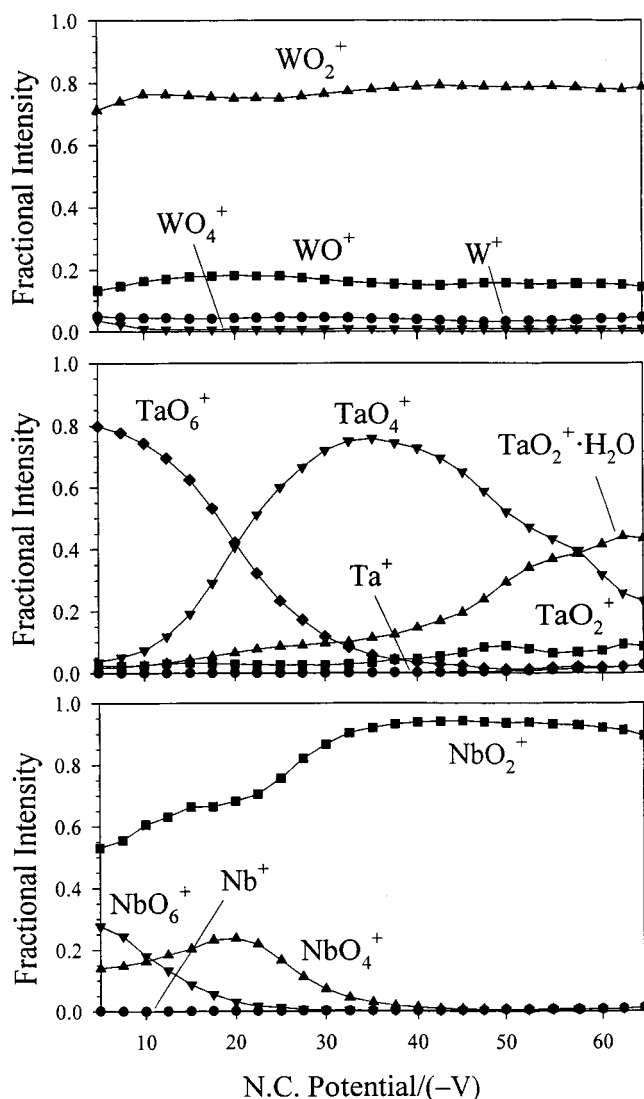
lision CID experiments indicated sequential loss of O_2 for the higher oxides (see Figure 6).

Unusual Formations of Higher Oxides. Experiments at very high flows of oxygen, up to 10^{20} molecules s^{-1}, were conducted with several ions. In the case of zirconium, rhenium, and osmium, these experiments revealed some unusual oxidation reactions.

With our experiments at high flows of oxygen, we have been able to track the sequential oxidation of Re$^+$ up to ReO$_6{}^+$ in the flow tube as indicated in Figure 7 (only trace amounts of ReO$_8{}^+$ were detected at very high flows). The observations shown in Figure 7 are consistent with the following reaction sequence

$$Re^+ + O_2 + He \rightarrow ReO_2{}^+ + He \quad (6)$$

$$ReO_2{}^+ + O_2 \rightarrow ReO_3{}^+ + O \quad (7a)$$

$$ReO_2{}^+ + O_2 + He \rightarrow ReO_4{}^+ + He \quad (7b)$$

$$ReO_3{}^+ + O_2 + He \rightarrow ReO_5{}^+ + He \quad (8)$$

$$ReO_4{}^+ + O_2 + He \rightarrow ReO_6{}^+ + He \quad (9)$$

A kinetic analysis using this scheme provides a reasonable fit to the observed ion profiles (see Figure 7) with the following (effective) bimolecular rate coefficients: $k_6 = 1.1 \times 10^{-12}$, $k_7 = 6.2 \times 10^{-11}$, $k_8 = 9.5 \times 10^{-12}$ and $k_9 = 1.9 \times 10^{-12}$ cm^3 molecule^{-1} s^{-1}. The branching ratio $k_{7a}/k_{7b} = 6:1$.

Figure 6. Multi-collision induced dissociation spectra for oxide cations of W, Ta and Nb. The flows of O_2 are 3.5×10^{17}, 1.1×10^{20} and 1.1×10^{20} cm^3 molecule^{-1} s^{-1}, respectively.

ReO$_x{}^+$ species ($x = 2-6$, 8) have been produced previously in a laser vaporization/supersonic expansion source, their reactivities have been explored using FT-ICR mass spectrometry, and their structures have been characterized by Beyer et al.[31,32] using FT-ICR CID techniques supplemented with calculations. Beyer et al. proposed a reaction scheme to explain the formation of all their observed oxides identical to that expressed by reactions 5 to 8. They suggested that the scheme is initiated by the direct oxidation of Re$^+$ with O_2 forming the Re(O_2)$^+$ isomer.[32] The reaction of the Re(O_2)$^+$ ion to form ReO$_3{}^+$ was computed by these authors to be exothermic by 79.8 kcal mol^{-1} and was shown to proceed in the FT-ICR experiments with 9% efficiency, in remarkable agreement with the value of 9.4% obtained with our experiments. No further kinetic information was obtained in the FT-ICR experiments, but it was proposed that Re(O_2)$^+$ also reacts with O_2 to initiate an O_2 addition sequence that ultimately forms Re(O_2)$_4{}^+$ and that ReO$_3{}^+$ forms ReO$_3$(O_2)$^+$. Beyer et al. also have provided theoretical insight into the structures and energies for all of these oxide ions.[32]
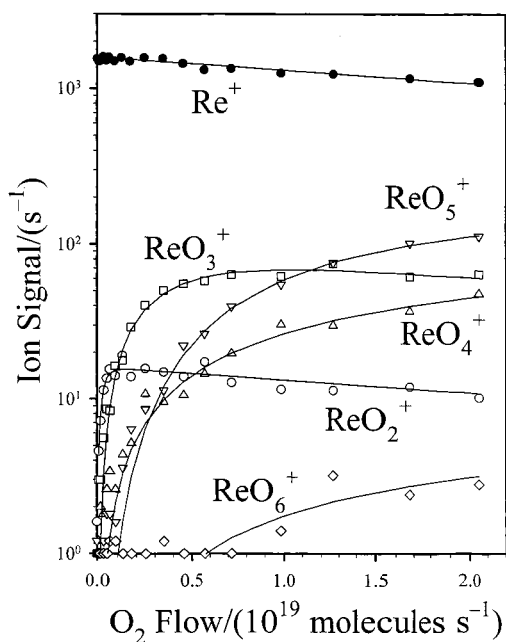
Figure 8 presents our ICP/SIFT observations made with Os$^+$ as the reacting ion that show the formation of the oxide ions OsO$_x{}^+$ ($x = 2-5$). Ground-state Os$^+$ appears to react slowly

RT Kinetics and Periodicities in Reactivity

J. Phys. Chem. A, Vol. 106, No. 18, 2002 **4589**

TABLE 5: Effective Bimolecular Rate Coefficients (in units of cm^3 molecule^{-1} s^{-1}) Measured for Some O$_2$ Addition Reactions of Transition-Metal Oxide Ions in Helium at 0.35 $\pm$ 0.01 Torr and 295 $\pm$ 2 K
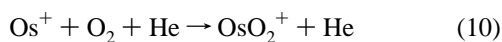
reaction	k	$k_{cap}{}^a$	k/k_{cap}
$TiO^+ + O_2 \rightarrow TiO_3^+$	$< 6 \times 10^{-13}$	6.4×10^{-10}	$<1 \times 10^{-3}$
$VO^+ + O_2 \rightarrow VO_3^+$	2.0×10^{-13}	6.3×10^{-10}	3.2×10^{-4}
$VO_3^+ + O_2 \rightarrow VO_5^+$	7.3×10^{-12}	6.0×10^{-10}	0.012
$VO_5^+ + O_2 \rightarrow VO_7^+$	2.0×10^{-12}	5.8×10^{-10}	3.4×10^{-3}
$YO^+ + O_2 \rightarrow YO_3^+$	1.0×10^{-11}	5.9×10^{-10}	0.017
$ZrO^+ + O_2 \rightarrow ZrO_3^+$	1.4×10^{-12}	5.9×10^{-10}	2.4×10^{-3}
$HfO^+ + O_2 \rightarrow HfO_3^+$	3.8×10^{-12}	5.6×10^{-10}	6.8×10^{-3}
$ReO_2^+ + O_2 \rightarrow ReO_3^+ + O$	6.2×10^{-11}	5.6×10^{-10}	0.11
$\quad \rightarrow ReO_4^+$			
$ReO_3^+ + O_2 \rightarrow ReO_5^+$	9.5×10^{-12}	5.6×10^{-10}	0.017
$OsO^+ + O_2 \rightarrow OsO_3^+$	2.8×10^{-12}	5.6×10^{-10}	5.0×10^{-3}
$OsO_3^+ + O_2 \rightarrow OsO_5^+$	1.3×10^{-11}	5.6×10^{-10}	0.023
	1.5×10^{-12}	6.1×10^{-10}	2.5×10^{-3}
$FeO_2^+ + O_2 \rightarrow FeO_4^+$	5.0×10^{-12}	6.1×10^{-10}	8.2×10^{-3}
$CoO_2^+ + O_2 \rightarrow CoO_4^+$	1.5×10^{-11}	6.1×10^{-10}	0.025
$NiO_2^+ + O_2 \rightarrow NiO_4^+$	1.7×10^{-12}	6.0×10^{-10}	2.8×10^{-3}
$CuO_2^+ + O_2 \rightarrow CuO_4^+$			
	4.2×10^{-13}	5.8×10^{-10}	7.2×10^{-4}
$NbO_2^+ + O_2 \rightarrow NbO_4^+$	1.9×10^{-12}	5.7×10^{-10}	3.3×10^{-3}
$NbO_4^+ + O_2 \rightarrow NbO_6^+$	4.1×10^{-12}	5.8×10^{-10}	7.1×10^{-3}
$MoO_2^+ + O_2 \rightarrow MoO_4^+$			
$RuO_2^+ + O_2 \rightarrow RuO_4^+$	1.3×10^{-12}	5.8×10^{-10}	2.2×10^{-3}
$RhO_2^+ + O_2 \rightarrow RhO_4^+$	3.2×10^{-13}	5.8×10^{-10}	5.5×10^{-4}
$HfO_2^+ + O_2 \rightarrow HfO_4^+$	2.4×10^{-13}	5.6×10^{-10}	4.2×10^{-4}
$TaO_2^+ + O_2 \rightarrow TaO_4^+$	6.4×10^{-13}	5.6×10^{-10}	1.1×10^{-3}
$TaO_4^+ + O_2 \rightarrow TaO_6^+$	2.7×10^{-11}	5.6×10^{-10}	4.8×10^{-3}
$WO_2^+ + O_2 \rightarrow WO_4^+$	2.4×10^{-12}	5.6×10^{-10}	4.3×10^{-3}
$ReO_4^+ + O_2 \rightarrow ReO_6^+$	1.9×10^{-12}	5.6×10^{-10}	3.4×10^{-3}
$OsO_2^+ + O_2 \rightarrow OsO_4^+$	2.1×10^{-11}	5.6×10^{-10}	0.038
$IrO_2^+ + O_2 \rightarrow IrO_4^+$	2.1×10^{-12}	5.6×10^{-10}	3.8×10^{-3}
$PtO_2^+ + O_2 \rightarrow PtO_4^+$	6.8×10^{-13}	5.6×10^{-10}	1.2×10^{-3}
$AuO_2^+ + O_2 \rightarrow AuO_4^+$	1.5×10^{-13}	5.6×10^{-10}	2.7×10^{-4}

^{a} Collision rate coefficient calculated using the algorithm of the modified variational transition-state/classical trajectory theory developed by Su and Chesnavich.[15]
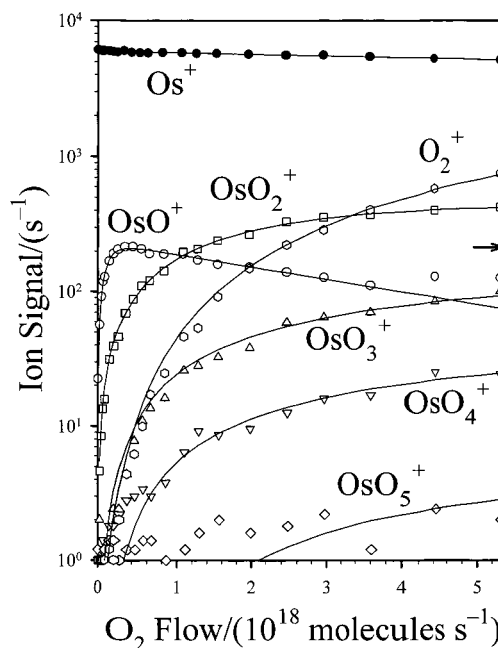

Figure 8. Chemistry initiated by Os$^+$ in oxygen. The data have been fit using sequential first-order kinetics for the mechanism described in the text. The arrow indicates the OsO$^+$ ion signal at a flow of 2.5 $\times$ 10^{19} molecules s^{-1}.

reaction of an excited state of Os$^+$ by O-atom transfer, reaction 11. Formation of the higher oxides can

$$(Os^+)^* + O_2 \rightarrow OsO^+ + O \tag{11}$$

then happen by the following O$_2$ addition reactions

$$OsO^+ + O_2 + He \rightarrow OsO_3^+ + He \tag{12}$$

$$OsO_2^+ + O_2 + He \rightarrow OsO_4^+ + He \tag{13}$$

$$OsO_3^+ + O_2 + He \rightarrow OsO_5^+ + He \tag{14}$$

Unusual Oxidation Reactions leading to Neutral Metal Oxides. A surprise encountered with the Os$^+$ chemistry is the formation of O$_2^+$ and OsO$^+$ at high flows of O$_2$ seen in Figure 8. We attribute the formation of these ions to the termolecular reactions 15a and 15b. These reactions will compete with

$$Os^+ + O_2 + O_2 \rightarrow O_2^+ + OsO_2 \tag{15a}$$

$$\rightarrow OsO^+ + O_3 \tag{15b}$$

reaction 10 because they all involve, as a first step, the formation of intermediate (OsO$_2^+$)* according to reaction 16. In reaction 10, this intermediate is stabilized by

$$Os^+ + O_2 \rightarrow (OsO_2^+)^* \tag{16}$$

collisions with He according to reaction 17, whereas in reaction

$$(OsO_2^+)^* + He \rightarrow OsO_2^+ + He \tag{17}$$

Figure 7. Chemistry initiated by Re$^+$ in oxygen. The data have been fit using sequential first-order kinetics for the mechanism described in the text.

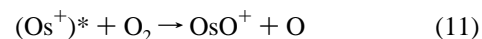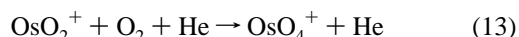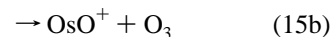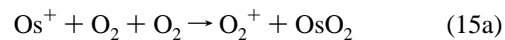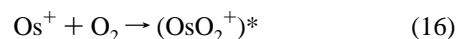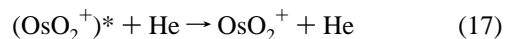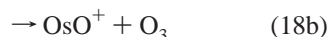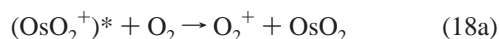with O$_2$ by addition to form OsO$_2^+$ according to reaction 9

$$Os^+ + O_2 + He \rightarrow OsO_2^+ + He \tag{10}$$

The early rise of small amounts of OsO$^+$ can be attributed to
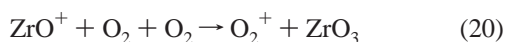
15a the intermediate receives an electron from O_2 according to reaction 18a and in reaction 15b the intermediate reacts with O_2 to form ozone according to reaction 18b.

$$(OsO_2^+)^* + O_2 \rightarrow O_2^+ + OsO_2 \quad (18a)$$

$$\rightarrow OsO^+ + O_3 \quad (18b)$$

Reaction 15a will be exothermic if $IE(Os) + D(Os-O_2) > IE(O_2)$ or if $D(Os-O_2) > 3.4$ eV or 78 kcal mol^{-1}. Unfortunately $D(Os-O_2)$ seems not to have been reported in the literature. Reaction 15b is exothermic by 6 kcal mol^{-1}. Reaction 15 is interesting because it may have generality for atomic or molecular ions, X^+ reacting with oxygen, reaction 19.

$$X^+ + O_2 + O_2 \rightarrow O_2^+ + XO_2 \quad (19a)$$

$$\rightarrow XO^+ + O_3 \quad (19b)$$

Reaction 19a will be exothermic if $IE(X) + D(X-O_2) > IE(O_2)$ and so would be favored for X species with high ionization energies and high O_2 affinities. Indeed, the appearance of O_2^+ in the zirconium experiment in Figure 3 is thought also to arise in this fashion according to reaction 20 which will compete with reaction 21.

$$ZrO^+ + O_2 + O_2 \rightarrow O_2^+ + ZrO_3 \quad (20)$$

$$ZrO^+ + O_2 + He \rightarrow ZrO_3^+ + He \quad (21)$$

Reaction 19b of course is favored by high $OA(X^+)$ but will be preempted by a direct O-atom transfer, reaction 1a, if $OA(X^+) > OA(O)$.

H$_2$O Addition to Oxide Ions. Water impurities in the helium buffer gas also were observed to add to some of the transition-metal oxide ions as illustrated in reaction 22. This is evident, for

$$MO_x^+ + H_2O + He \rightarrow MO_x^+ \cdot H_2O + He \quad (22)$$
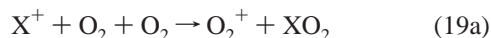
example, in the data for the monoxide ions YO^+ and ZrO^+ (see Figure 3), the dioxide ions MoO_2^+ (see Figure 3) and TaO_2^+ (see Figure 4) and the trioxide ion YO_3^+ (see Figure 3).

Conclusions

The ICP/SIFT tandem mass spectrometer has provided a full measure of the reactivity of transition-metal ions with molecular oxygen. The two observed reaction channels, O-atom abstraction and O_2 addition, have a periodic dependence that exhibits a strong correlation with the O-atom affinities of the metal ions. Early transition-metal ions exhibit efficient O-atom abstraction, whereas late transition-metal ions prefer to simply add O_2.

Further O-atom abstraction proceeds with NbO^+, MoO^+, TaO^+, and WO^+ to form dioxide cations and with ReO_2^+ and OsO_2^+ produced by direct addition of O_2 to Re^+ and Os^+ to produce trioxide cations.

Sequential O_2 addition was observed to produce still higher oxides: MO_3^+ (M = Ti, V, Y, Zr), MO_4^+ (M = Cr, Fe, Co, Ni, Cu, Nb, Mo, Ru, Rh, Ta, W, Re, Os, Ir, Pt, Au), MO_5^+ (M = V, Re, Os), MO_6^+ (M = Nb, W, Re) and MO_7^+ (M = V).

A novel termolecular reaction second-order in oxygen was identified for Os^+ and ZrO^+ at high oxygen concentrations to produce O_2^+ and a neutral metal oxide. These reactions may be prototypes for a more general reaction type.

Note Added after Print Publication: Due to a production error, an incorrect version of Figure 4 was published on the Web 4/3/2002 (ASAP) and in the May 9, 2002 issue (Vol. 106, No. 18, pp 4581−4590); the correct electronic version of the paper was published on 5/15/2002.

References and Notes

(1) See for example, D. Schröder; H. Schwarz; S. Shaik In. *Structure and Bonding*; Springer-Verlag: Berlin Heidelberg, 2000**,** Vol. 97, p 91.
(2) Johnson, R.; Castell, F. R.; Biondi, M. A. *J. Chem. Phys.* **1974**, *61*, 5404.
(3) Dheandhanoo, S.; Chatterjee, B. K.; Johnson, R. *J. Chem. Phys.* **1985**, *83*, 3327.
(4) Kappes, M. M.; Staley, R. H. *J. Phys. Chem.* **1981**, *85*, 942.
(5) Fisher, E. R.; Elkind, J. L.; Clemmer, D. E.; Georgiadis, R.; Loh, S. K.; Aristov, N.; Sunderlin, L. S.; Armentrout, P. B. *J. Chem. Phys.* **1990**, *93,* 942.
(6) Koyanagi, G. K.; Lavrov, V..; Baranov, V. I.; Bandura, D.; Tanner, S. D.; McLaren, J. W.; Bohme, D. K. *Int. J. Mass Spectrom.* **2000**, *194*, L1.
(7) Koyanagi, G. K.; Baranov, V. I.; Tanner, S. D.; Bohme, D. K. *J. Anal. At. Spectrom.* **2000**, *15*, 1207.
(8) Koyanagi, G. K.; Bohme, D. K. *J. Phys. Chem. A* **2001**, *105*, 8964.
(9) Mackay, G. I.; Vlachos, G. D.; Bohme, D. K.; Schiff, H. I. *Int. J. Mass Spectrom. Ion Phys.* **1980**, *36*, 259.
(10) Raksit, A. B.; Bohme, D. K. *Int. J. Mass Spectrom. Ion Processes* **1983/84**, *55*, 69.
(11) Moore, C. E. Atomic Energy Levels as Derived from the Analyses of Optical Spectra; U.S. National Bureau of Standards: Washington, 1971.
(12) Van Kleef, Th. A. M.; Metsch, B. C. *Physica* **1978**, *C 95*, 251.
(13) Koyanagi, G. K.; Bohme, D. K.; Kretzschmar, I.; Schröder, D.; Schwarz, H. *J. Phys. Chem. A* **2001**, *105*, 4259.
(14) Lias, S. G.; Bartmess, J. E.; Liebman, J. F.; Holmes, J. L.; Levin, R. D.; Mallard, W. G. *J. Phys. Chem. Ref. Data* **1988**, *17*: Suppl 1.
(15) Su, T.; Chesnavich, W. J. *J. Chem. Phys.* **1982**, *76*, 5183.
(16) Freiser, B. S., Ed. *Organnometallic Ion Chemistry*; Kluwer: Dordrecht, 1996.
(17) Sievers, M. R.; Chen, Y.-M.; Armentrout, P. B. *J. Chem. Phys.* **1996**, *105*, 6322.
(18) Chen, Y.-M.; Armentrout, P. B. *J. Chem. Phys.* **1995**, *103*, 618.
(19) Clemmer, D. E.; Dalleska, N. F.; Armentrout, P. B. *Chem. Phys. Lett.* **1992**, *190,* 259.
(20) Beyer, M. Dissertation, Technical University München, 1966.
(21) Irikura, K. K.; Beauchamp, J. L. *J. Am. Chem. Soc.* **1989**, *111*, 75.
(22) Pavlov, M.; Blomberg, M. R. A.; Siegbahn, P. E. M.; Wesendrup, R.; Heinemann, C.; Schwarz, H. *J. Phys. Chem. A* **1997**, *101*, 1567.
(23) Baranov, V. I.; Bohme, D. K. *Int. J. Mass Spectrom. Ion Processes* **1996**, *154*, 71.
(24) Harvey, J. N.; Diefenbach, M.; Schröder, D.; Schwarz, H. *Int. J. Mass Spectrom.* **1999**, *182/183*, 85.
(25) Sievers, M. R.; Armentrout, P. B. *Int. J. Mass Spectrom.* **1999**, *185/186/187*, 117.
(26) Kretzschmar, I.; Fiedler, A.; Harvey, J. N.; Schröder, D.; Schwarz, H. *J. Phys. Chem. A* **1997**, *101*, 6252.
(27) Sievers, M. R.; Armentrout, P. B. *J. Phys. Chem. A* **1998**, *102*, 10 754.
(28) Schröder, D.; Fiedler, A.; Schwarz, J.; Schwarz, H. *Inorrg. Chem.* **1994**, *33*, 5094.
(29) Fiedler, A.; Kretzschmar, I.; Schröder, D.; Schwarz, J.; Schwarz, H. *J. Am. Chem. Soc.* **1996**, *118*, 9941.
(30) Brönstrup, M.; Schröder, D.; Kretzschmar, I.; Schwarz, H.; Harvey, J. N. *J. Am. Chem. Soc.* **2001**, *123*, 142.
(31) Beyer, M.; Berg, C.; Albert, G.; Achatz, U.; Joos, S.; Niedner-Schatteburg, G.; Bondybey, V. *J. Am. Chem. Soc.* **1997**, *119*, 1466.
(32) Beyer, M.; Berg, C.; Albert, G.; Achatz, U.; Hieringer, W.; Niedner-Schatteburg, G.; Bondybey, V. *Int. J. Mass Spec.* **1999**, *185/186/187*, 625.